Macromolecular Rapid Communications
www.mrc-journal.de

Highly Thermally Stable, Reversible, and Flexible Main Chain Type Benzoxazine Hybrid Incorporating Both Polydimethylsiloxane and Double-Decker Shaped Polyhedral Silsesquioxane Units through Diels–Alder Reaction

*Cheng-Yu Chen, Wei-Cheng Chen, Mohamed Gamal Mohamed, Zih-Yu Chen, and Shiao-Wei Kuo**

This work synthesizes a new bifunctional furan derivative (PDMS-FBZ) through a sequence of hydrosilylation of nadic anhydride (ND) with polydimethylsiloxane (PDMS), reaction of the product with *p*-aminophenol to form PDMS-ND-OH, and its subsequent Mannich reaction with furfurylamine and CH_2O. Then, the main chain-type copolymer PDMS-DABZ-DDSQ is prepared through a Diels–Alder (DA) cycloaddition of PDMS-FBZ with the bismaleimide-functionalized double-decker silsesquioxane derivative DDSQ-BMI. Fourier transform infrared (FTIR) and nuclear magnetic resonance (NMR) spectroscopy confirm the structure of this PDMS-DABZ-DDSQ copolymer; differential scanning calorimetry (DSC), thermogravimetric analysis (TGA), and dynamic mechanical analysis (DMA) reveal it to have high flexibility and high thermal stability (T_g = 177 °C; T_{d10} = 441 °C; char yield = 60.1 wt%); contact angle measurements reveal a low surface free energy (18.18 mJ m^{-2}) after thermal ring-opening polymerization, because the inorganic PDMS and DDSQ units are dispersed well, as revealed using scanning electron microscopy (SEM) and transmission electron microscopy (TEM). This PDMS-DABZ-DDSQ copolymer possesses reversible properties arising from the DA and retro-DA reactions, suggesting its possible application as a functional high-performance material.

1. Introduction

Benzoxazine (BZ) resins, thermosetting resins featuring six-membered heterocyclic rings, possess many superior physical and chemical properties (e.g., a stable dielectric constant, high thermal and dimensional stabilities, low surface free energy, and good flame retardancy), relative to those of traditional phenolic and epoxy resins,[1–6] because strong intramolecular hydrogen bonding of their OH···N units occurs after thermal polymerization to form three-dimensional cross-linked structures.[7,8] BZ resins are usually synthesized from a phenolic derivative, CH_2O, and a primary aliphatic or aromatic amine in a solvent or without a solvent. Nevertheless, BZ resin has limited applicability at high temperature since C–N–C bond of molecule with no cross-links is readily broken at temperature >260 °C.[9] Attempts have been made to decrease chain mobility of BZ resin to improve its thermal and mechanical properties by incorporating unsaturated (such as allyl or alkynyl) groups, blending with high-performance polymers to form miscible blends,[10–16] and adding inorganic nanoparticles.[17–22]

Many organic/inorganic polybenzoxazine (PBZ) hybrids (and other thermosetting resins) have been prepared by incorporating carbon-based materials (e.g., carbon nanotubes,[23–25] carbon black,[26] and graphene[27–30]) and silicon-based materials [e.g., polydimethylsiloxane (PDMS),[5,31–33] organic modified clay,[34,35] and polyhedral oligomeric silsesquioxane (POSS)[17–22,36–40]]. For example, polymer/POSS hybrids have been obtained from mono- and multifunctionalized POSS derivatives through blending or copolymerization, initially forming organic/inorganic hybrids with only relatively low-molecular-weight or insoluble cross-linked structures.[36–39] Accordingly, main chain-type PBZs have been reacted with difunctionalized POSS cages to form high-molecular-weight and soluble hybrids. For instance, Zheng et al. reacted a diamine-substituted double-decker silsesquioxane with bisphenol A and CH_2O to obtain the main chain type of PBZ/DDSQ hybrids.[22] Furthermore, we have previously prepared a flexible and transparent PBZ copolymer, featuring silicon-based flexible PDMS and rigid DDSQ units, through the Mannich condensation of allyl amine with the bifunctionalized phenolic DDSQ and CH_2O and then subsequent hydrosilylation with PDMS; after thermal polymerization of its BZ monomer units, the resulting main chain-type PBZ copolymer PDMS-BZ-DDSQ did not display the brittleness usually observed for typical PBZs.[21]

C.-Y. Chen, W.-C. Chen, M. G. Mohamed, Z.-Y. Chen, S.-W. Kuo
Department of Materials and Optoelectronic Science, Center for Functional Polymers and Supramolecular Materials
National Sun Yat-Sen University
Kaohsiung 80424, Taiwan
E-mail: kuosw@faculty.nsysu.edu.tw

The ORCID identification number(s) for the author(s) of this article can be found under https://doi.org/10.1002/marc.202200910

DOI: 10.1002/marc.202200910

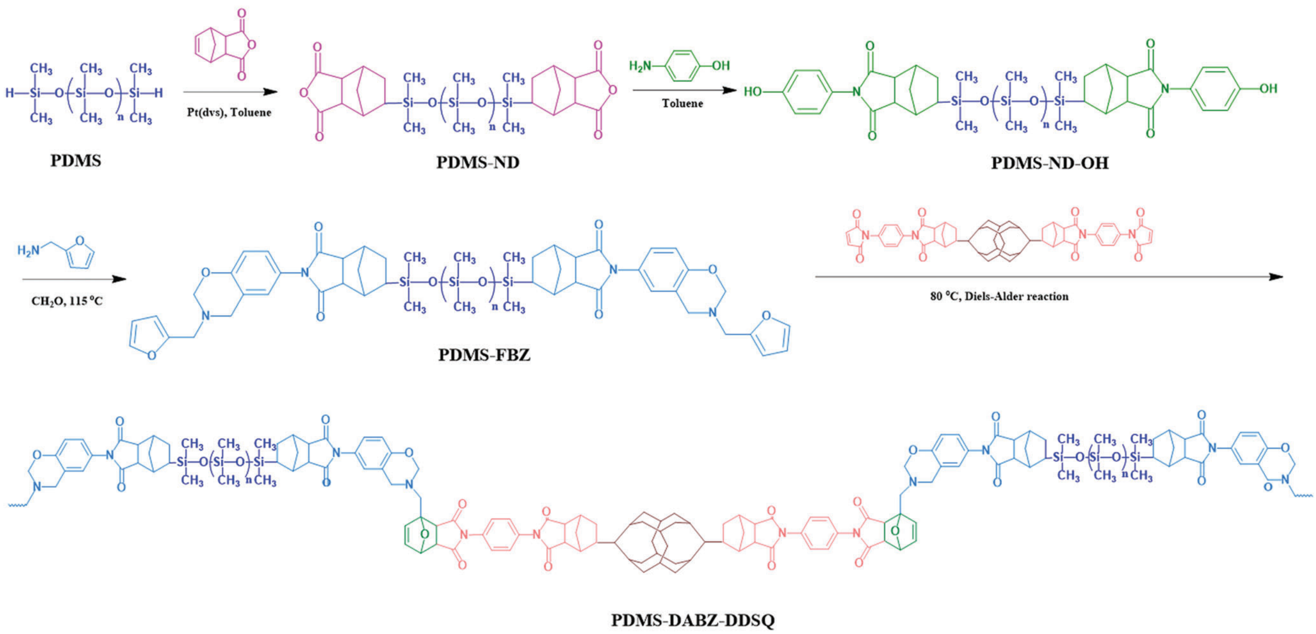

Scheme 1. Synthesis of PDMS-FBZ from polydimethylsiloxane (PDMS), PDMS-ND, and PDMS-ND-OH reacting with furfurylamine and CH_2O and then react with DDSQ-BMI to form PDMS-DABZ-DDSQ.

In this study, we used Diels–Alder (DA) cycloadditions of a furan-functionalized PDMS BZ monomer [PDMS-FBZ] and a bismaleimide-functionalized DDSQ monomer [DDSQ-BMI] to form a new main chain-type PDMS-DABZ-DDSQ copolymer (**Scheme 1**). This newly synthesized BZ undergoes reversible DA reaction, as investigated widely by the Zhang group,[41] suggesting chemical recycling properties. Because our resulting organic/inorganic PBZ hybrid possessed flexible PDMS and rigid DDSQ inorganic nanomaterials, it displayed high thermal stability, flexibility, and a low surface energy, indicating its potential for application as a high-performance material.

2. Results and Discussion

2.1. Synthesis, Thermal Polymerization, and Surface Free Energy of PDMS-FBZ Monomer

Scheme 1 presents our synthesis of the PDMS-FBZ monomer from the hydride-terminated PDMS. The PDMS derivatives synthesized in this study were all characterized using FTIR and NMR spectroscopy (**Figure 1**). First, we synthesized a material presenting bifunctionalized phenolic groups through hydrosilylation of ND with the hydride-terminated PDMS. We then reacted PDMS-ND with *para*-aminophenol to form PDMS-ND-OH. Finally, we prepared PDMS-FBZ by reacting PDMS-ND-OH with furfurylamine and CH_2O in 1,4-dioxane at 115 °C for 72 h. Figure 1a displays the FTIR spectrum of each PDMS derivative during the preparation of PDMS-FBZ. Two strong absorptions at 1254 (Si–CH_3 units) and 1092 (Si–O–Si unit) cm^{-1} appeared for each PDMS derivative. The spectrum of the pure PDMS featured a signal for the Si–H unit at 2130 cm^{-1}; after hydrosilylation of ND, this signal disappeared and two new signals for the C=O groups of the anhydride units appeared at 1861 and 1779 cm^{-1}, consistent with the formation of PDMS-ND. The spectrum of PDMS-ND-OH featured a broad O–H stretching band at 3380 cm^{-1} and signals for imide C=O stretching that had shifted to lower wavenumbers (1780 and 1699 cm^{-1}). The FTIR spectrum of PDMS-FBZ features signals for the oxazine ring at 932 cm^{-1} and the furan ring at 1498 cm^{-1}, but no signal for O–H stretching. Figure 1b and Figure S1 (Supporting Information) present the ^1H NMR spectra of each PDMS derivative; Figure 1 summarizes the peak assignments. The spectrum of PDMS featured signals for the SiH and Si–CH_3 protons at 4.70 and 0.16 ppm, respectively. The signal for the SiH protons disappeared after the hydrosilylation forming PDMS-ND, with two isomers present, with α- and β-configurations, as revealed by signals for those aliphatic protons between 0.64 and 3.41 ppm; no signals for residual vinyl were evident. The spectrum of PDMS-ND-OH featured signals for the phenolic OH groups at 8.03 ppm and aromatic protons (derived from aminophenol) at 7.08 (a) and 6.88 ppm (b). The signal for the phenolic OH groups was absent from the spectrum of PDMS-FBZ; signals for the oxazine ring at 4.86 (c, OCH_2N) and 3.94 (d, $ArCH_2N$) ppm (≈1:1 integral area), a signal at 3.84 ppm representing the furyl-CH_2N (e) group, and three other signals at 6.29, 6.38, and 7.60 ppm for the furyl unit confirmed the synthesis of this new PDMS-FBZ monomer with high purity.

Figure 2a displays DSC profiles of the cured PDMS-FBZ. The thermal ring-opening polymerization (ROP) at 235 °C occurred with a reaction enthalpy of 31.3 J g^{-1}—a value lower than that of a typical Pa-type monomer (263 °C) because of the catalytic effect of the furyl units.[42,43] Upon increasing the thermal ROP temperature from 100 °C, the signal for exothermic thermal curing gradually disappeared; it disappeared completely at 250 °C, indicating the formation of poly(PDMS-FBZ) (Figure 2a). We used FTIR spectroscopy to investigate the thermal ROP behavior of PDMS-FBZ at each temperature (Figure 2b). The intensity of the

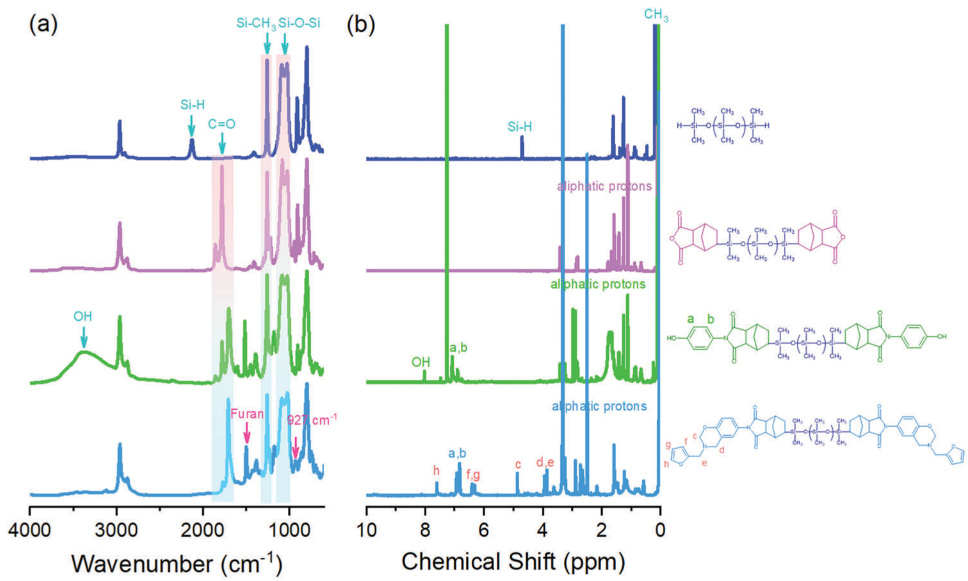

Figure 1. a) Fourier transform infrared (FTIR) and b) ^{1}H nuclear magnetic resonance (NMR) spectra of polydimethylsiloxane (PDMS), PDMS-ND, PDMS-ND-OH, and PDMS-FBZ.

signal at 932 cm^{-1} decreased upon increasing thermal ROP temperature, disappearing completely at 250 °C (Figure 2c), consistent with the DSC thermal analyses. We measured the char yield and 10% weight loss temperature (T_{d10}) to investigate the thermal stability of the PDMS-FBZ monomer after ROP at each temperature (Figure 2d), based on TGA analysis. The uncured PDMS-FBZ monomer provided a value of T_{d10} at 277 °C and a char yield of 19.4 wt% at 800 °C. After thermal ROP treatment at 100 °C, 150 °C, 200 °C, and 250 °C, its values of T_{d10} were 268 °C, 285 °C, 354 °C, and 435 °C, respectively, and its char yields were 20.8, 21.9, 28.3, and 43.5 wt%, respectively. The value of T_{d10} and the char yield of poly(PDMS-FBZ) after thermal ROP at 250 °C were remarkable relative to those of the Pa-type BZ (≈320 °C and 35 wt%, respectively). This superior thermal stability was presumably due to the presence of inorganic PDMS units and the additional cross-linking arising from the furan units. Figure 2e displays DMA thermal analyses of poly(PDMS-FBZ) after thermal ROP at 250 °C. The initial storage modulus at 25 °C was 575 MPa. The loss tan δ peak provided a value of T_g of 110°; this value is lower than that of a typical poly(Pa-BZ) after thermal ROP (138 °C), as we had expected after incorporation of flexible inorganic PDMS units into the PBZ matrix (Figure 2f).

We used CA analyses to investigate the surface properties of PDMS-FBZ before and after thermal ROP (Figure S2, Supporting Information). We calculated the surface free energies (γ_s) from the CAs of H_2O (Figure S2a, Supporting Information), EG (Figure S2b, Supporting Information), and CH_2I_2 (Figure S2c, Supporting Information) measured after ROP from room temperature to 250 °C; in previous studies, we found that these values were strongly dependent on the degree of intramolecular hydrogen bonding of OH···N units after thermal ROP.[44,45] The surface free energies of these poly(PDMS-FBZ) films decreased from 37.68 mJ m^{-2} after ROP at 25 °C to 13.68 mJ m^{-2} after ROP at 250 °C), based on the Owens–Wendt–Rabel–Kaelble (OWRK) method (Figure S2d, Supporting Information). The value of 13.68 mJ m^{-2} is much lower than those of typical BA-m– or BA-a–type PBZs after thermal ROP (16.4 and 19.2 mJ m^{-2}, respectively), suggesting the presence of strong intramolecular OH···N hydrogen bonding.[44] The inorganic flexible PDMS segments provided additional hydrophobicity to the PBZ matrix, as expected.[46,47]

2.2. Synthesis, Thermal Polymerization, and Surface Free Energy of PDMS-DABZ-DDSQ Copolymer

To further increase the thermal and mechanical properties of PDMS-FBZ, we incorporated rigid inorganic DDSQ-BMI to form a main chain-type PDMS-DABZ-DDSQ copolymer through DA cycloaddition (Scheme 1). **Figure 3**a displays the FTIR spectra of PDMS-FBZ, DDSQ-BMI, and PDMS-DABZ-DDSQ recorded at room temperature. After DA cycloaddition, we observed signals for Si–O–Si moieties from both the PDMS and DDSQ units near 1137 and 1084 cm^{-1}, the C=O groups from the PDMS-FBZ and DDSQ-BMI units near 1717 cm^{-1}, and the oxazine rings from the PDMS-FBZ unit at 932 cm^{-1}, confirming the formation of the PDMS-DABZ-DDSQ copolymer. Figure 3b and Figure S3 (Supporting Information) present the ^{1}H NMR spectra of PDMS-FBZ, DDSQ-BMI, and the PDMS-DABZ-DDSQ copolymer. In the latter, signals for the two methylene units of the oxazine ring appeared at 4.87 (a, NCH_2O) and 4.00 (b, $ArCH_2N$) ppm. Furthermore, the formation of the DA adduct was evident from signals at 6.00, 5.31, and 3.86 ppm corresponding to protons H_h, H_c, and H_i, respectively. The PDMS-DABZ-DDSQ copolymer displayed good solubility in common organic solvents (e.g., DMF, NMP, DMSO, THF). Thus, this main chain-type copolymer was readily processable through solvent casting to form free-standing films, and we could also check its molecular weight through size exclusion chromatography (SEC; M_n = 9200 g mol^{-1}; PDI = 1.55). Figure 3e presents the thermomechanical properties of the PDMS-DABZ-DDSQ copolymer, as determined through DMA

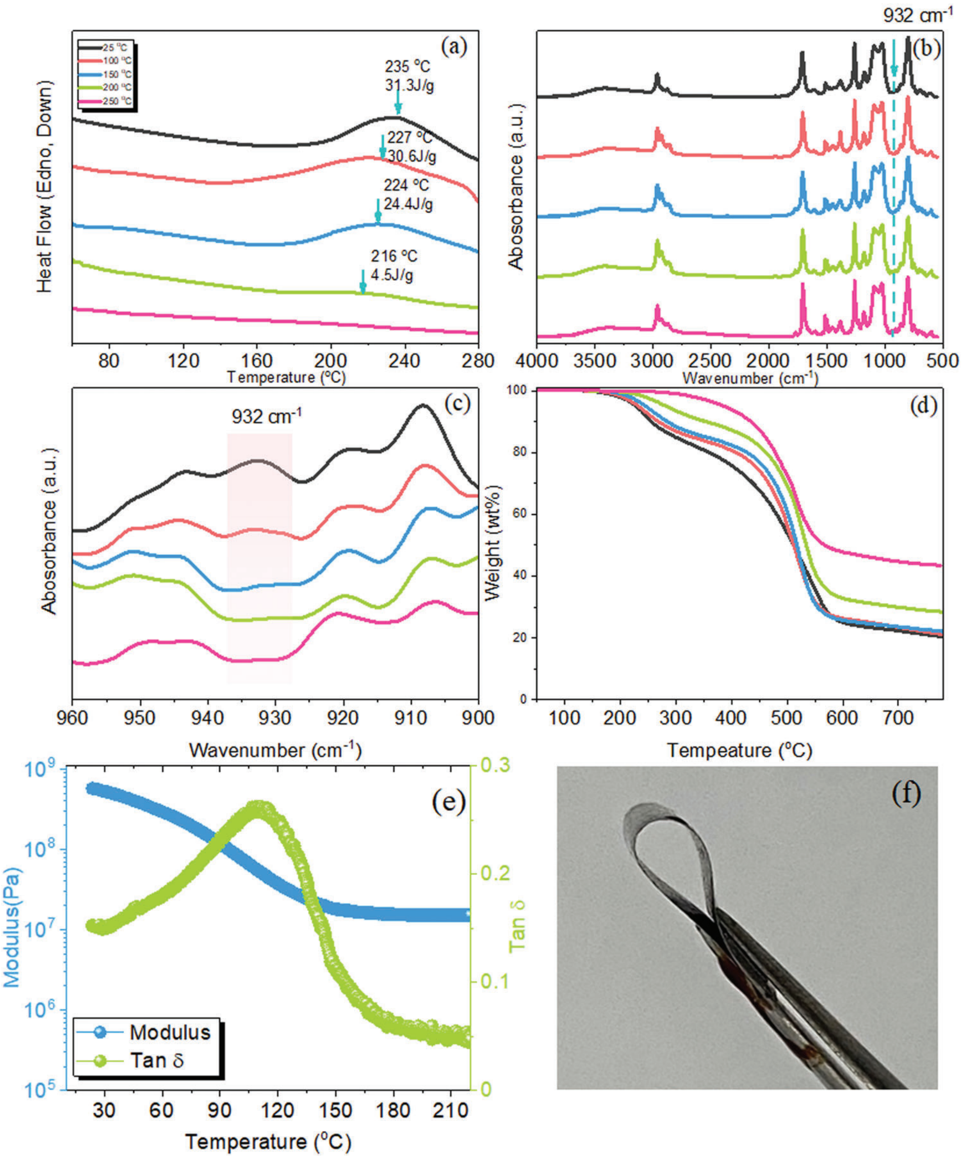

Figure 2. a) Differential scanning calorimetry (DSC) thermal analyses, b,c) Fourier transform infrared (FTIR) spectra, and d) thermogravimetric analysis (TGA) analysis of the PDMS-FBZ-monomer after thermal polymerization at various temperatures. e) Dynamic mechanical analysis (DMA) analysis and f) photograph of a flexible film of PDMS-BZ after thermal polymerization at 250 °C.

analysis; the value of T_g determined from loss tan δ peak was 44 °C and the initial storage modulus at 25 °C was 313 MPa, suggesting reasonable film properties in the absence of thermal ROP. Figure 3f and Figure S4b (Supporting Information) display TEM and SEM images of the PDMS-DABZ-DDSQ copolymer, revealing the dispersion of the inorganic PDMS and DDSQ components. The featureless morphology, without macrophase separation, suggests that the PDMS and DDSQ units were dispersed homogeneously in the copolymer matrix. Furthermore, C, Si, N, and O mappings, based on SEM analyses (Figure S4c–f, Supporting Information), revealed the uniform presence of Si atoms, suggesting that the PDMS and DDSQ units were both dispersed well in the copolymer. Thus, all of the characterization data indicated the successful synthesis of the main chain-type PDMS-DAB Z-DDSQ copolymer. We also employed DSC and TGA analyses (Figure 3c,d) to investigate the thermal ROP of our main chain-type PDMS-DABZ-DDSQ copolymer. As mentioned above, the uncured PDMS-FBZ underwent thermal ROP at 235 °C, with a broad exothermic peak (289 °C) observed in Figure 3c corresponding to the addition–polymerization of pure DDSQ-BMI.[40] The broad maximum exothermic peak of the PDMS-DABZ-DDSQ copolymer appeared at 230 °C, slightly lower than that of PDMS-FBZ, due to thermal cross-linking polymerization. Furthermore, a broad complex endothermic signal appeared near 135 °C, corresponding to the retro-DA reaction; thus, cleavage of the DA cycloaddition products, induced through a thermoresponsive reaction, presumably generated new polymerizable and reactive functional units (e.g., maleimide and furan units).[48–51] In addition, the olefinic double bond from the uncleaved DA adduct might also have participated in the thermal

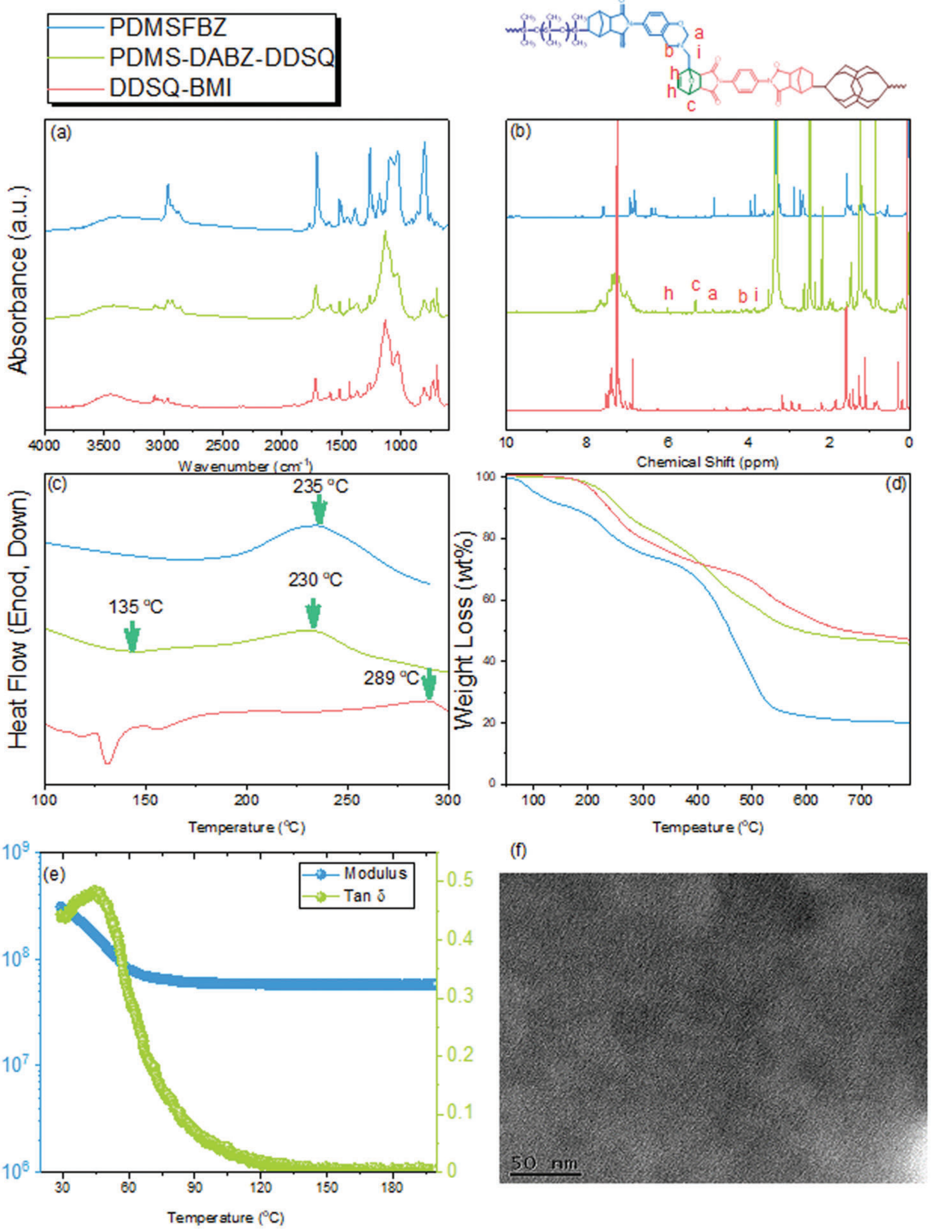

Figure 3. a) Fourier transform infrared (FTIR) and b) ^{1}H nuclear magnetic resonance (NMR) spectra, c) differential scanning calorimetry (DSC), and d) thermogravimetric analysis (TGA) thermal analyses of PDMS-DABZ-DDSQ derived from PDMS-FBZ and DDSQ-BMI, e) dynamic mechanical analysis (DMA) thermal analyses and f) transmission electron microscopy (TEM) image of PDMS-DABZ-DDSQ recorded prior to thermal polymerization.

ROP with the maleimide or furan units upon further thermal heating. **Scheme 2** provides a plausible mechanism for the thermal ROP of the PDMS-DABZ-DDSQ copolymer to form a highly cross-linked structure for poly(PDMS-DABZ-DDSQ).

Figure 3d displays the TGA traces of PDMS-FBZ, DDSQ-BMI, and the PDMS-DABZ-DDSQ copolymer, recorded before thermal ROP under a N_2 atmosphere. As revealed in Figure 2d, the uncured PDMS-FBZ monomer provided a value of T_{d10} and a char yield of 169 °C and 20.1 wt%, respectively; for the DDSQ-BMI used in this study, these values were 237 °C and 47.1 wt%, respectively. The main chain-type PDMS-DABZ-DDSQ copolymer displayed a higher value of T_{d10} of 258 °C, because covalent bonding between PDMS-FBZ and DDSQ-BMI could increase the thermal decomposition temperature; its char yield of 45.7 wt% was, as expected, slightly lower than that of DDSQ-BMI, because the copolymer possessed a PDMS segment of relatively lower char yield.

Figure 4a displays DSC traces of the PDMS-DABZ-DDSQ copolymer, recorded before and after thermal ROP at various temperatures. The reaction enthalpy and the intensity of the thermal ROP peak both decreased upon increasing the thermal ROP temperature, disappearing completely at 250 °C; FTIR spectral analyses confirmed these phenomena, with the signal of the oxazine ring at 932 cm^{-1} decreasing upon increasing the

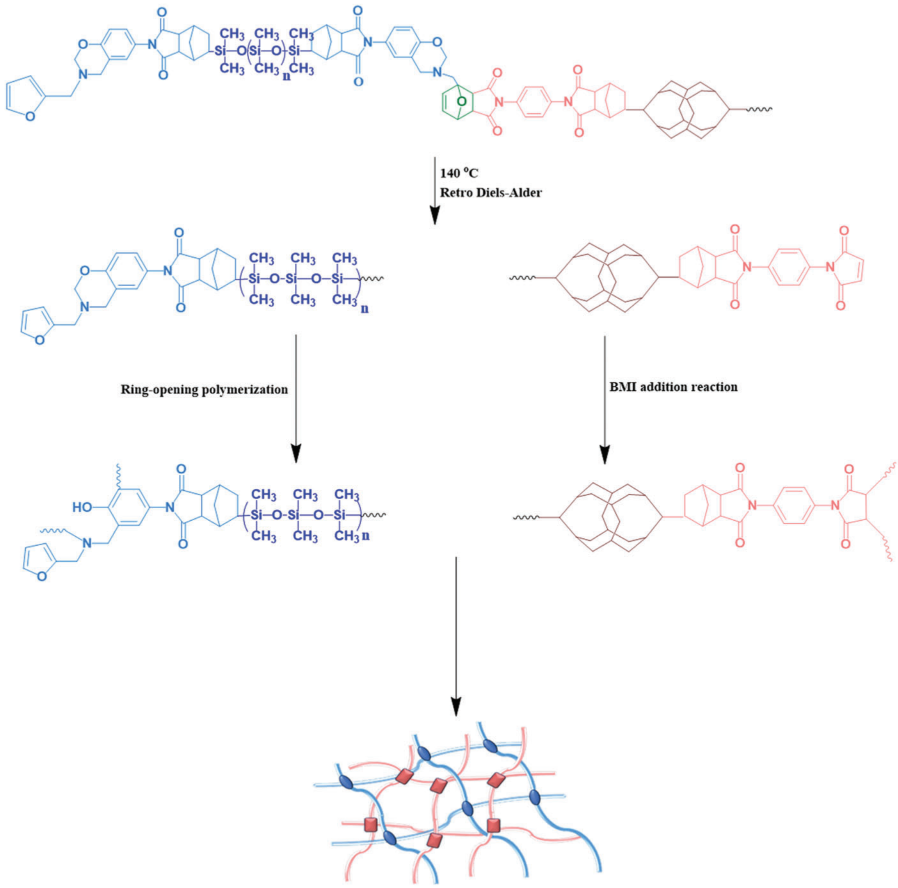

Scheme 2. Possible mechanism of thermal polymerization of PDMS-DABZ-DDSQ to form poly(PDMS-DABZ-DDSQ).

ROP temperature and also disappearing completely after ROP at 250 °C (Figure 4b). Figure 4c presents the corresponding TGA analyses of the PDMS-DABZ-DDSQ copolymer before and after thermal ROP at the various temperatures. The uncured PDMS-DABZ-DDSQ copolymer provided a value of T_{d10} and a char yield of 237 °C and 47.1 wt%, respectively (Figure 4c). Interestingly, after its thermal ROP treatment at 100 °C and 150 °C, the values of T_{d10} decreased to 230 °C and 223 °C, respectively, and the char yields decreased to 42.7 and 37.8 wt%, respectively. This phenomenon has rarely been observed for BZ monomers during thermal ROP; it can be explained by considering that retro-DA reactions occurred at these temperatures, with cleavage of the DA cycloadducts reforming maleimide and furan units (Scheme 2) and leading to relatively lower values of T_{d10} and char yield. Further increasing the ROP temperature to 200 and 250°C caused the values of T_{d10} to increase to 369 and 441°C, respectively, and the char yields to increase to 55.6 and 60.1 wt%, respectively. Figure 4d provides the DMA thermal analysis of the PDMS-DABZ-DDSQ copolymer after thermal ROP at 250°C. The loss tan δ peak corresponded to a value of T_g of 177°C. The values of T_g and T_{d10} and the char yield for poly(PDMS-DABZ-DDSQ) (177 °C, 441 °C, and 60.1 wt%, respectively) were all significantly higher than those for poly(PDMS-FBZ) (110 °C, 435 °C, and 43.5 wt%, respectively) after thermal ROP at 250 °C, presumably because the rigid inorganic DDSQ cage structures were dispersed well in the former copolymer hybrid to enhance its thermal stability and also displays flexible behavior as also shown in Figure 4d.

Figure 5a,b presents TEM and SEM images of the poly(PDMS-DABZ-DDSQ) hybrid after thermal ROP at 250 °C, recorded to investigate the dispersion of its inorganic PDMS and DDSQ units. The featureless morphology, without macrophase separation, suggests that the PDMS and DDSQ units were dispersed homogeneously in the hybrid matrix. Furthermore, the C, Si, N, and O mappings, based on SEM analyses (Figure 5c–f), also revealed the uniform dispersion of the Si atoms from both the PDMS and DDSQ units in the copolymer. As a result, this new poly(PDMS-DABZ-DDSQ) hybrid is also much more thermally stable than the polymers formed from the typical Pa-type BZ (T_g = 130 °C; T_{d10} = 320 °C; char yield = 35.0 wt%), while also featuring flexibility and reversible properties.

Figure S5 (Supporting Information) displays the surface properties of PDMS-DABZ-DDSQ before and after thermal ROP, as determined from the CAs of H_2O (Figure S5a, Supporting Information), EG (Figure S5b, Supporting Information), and CH_2I_2 (Figure S5c, Supporting Information) measured after thermal treatment from room temperature to 250 °C. The surface free energies of these poly(PDMS-DABZ-DDSQ) films decreased from 30.86 after treatment at 25 °C to 18.18 mJ m^{-2} after treatment at 250 °C, based on the OWRK method (Figure S5d). The surface free energies of the poly(PDMS-DABZ-DDSQ) films were

Macromolecular Rapid Communications
www.mrc-journal.de

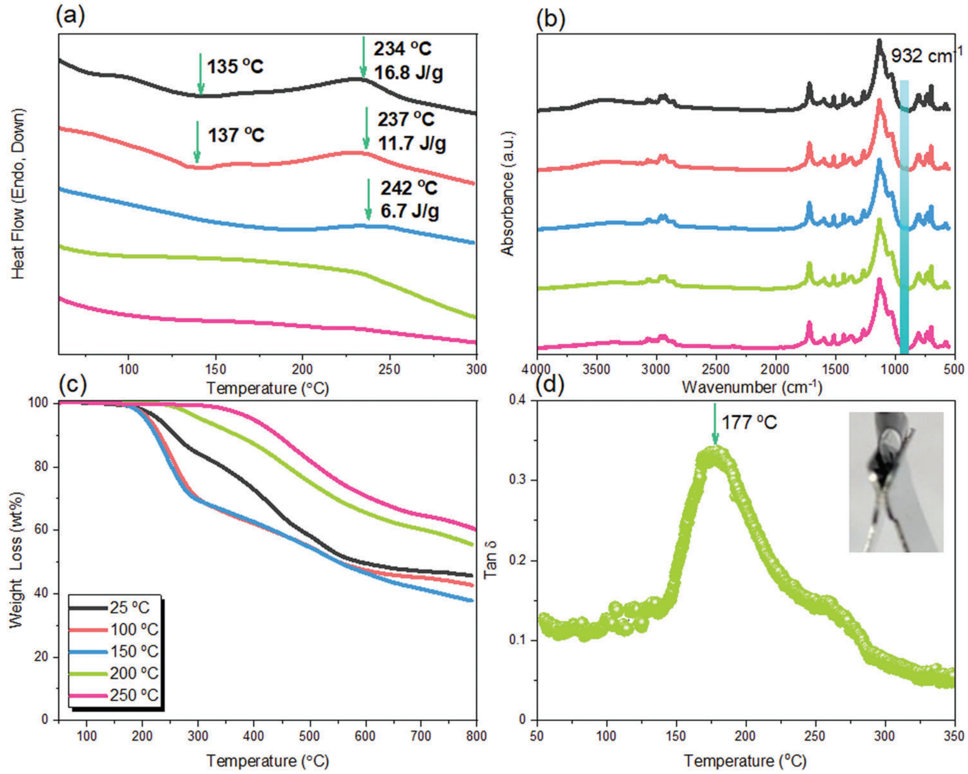

Figure 4. a) Differential scanning calorimetry (DSC) thermal analyses, b) Fourier transform infrared (FTIR) spectra, and c) thermogravimetric analysis (TGA) analyses of PDMS-DABZ-DDSQ after thermal polymerization at various temperatures. d) Dynamic mechanical analysis (DMA) analysis and a flexible film of PDMS-DABZ-DDSQ after thermal polymerization at 250 °C.

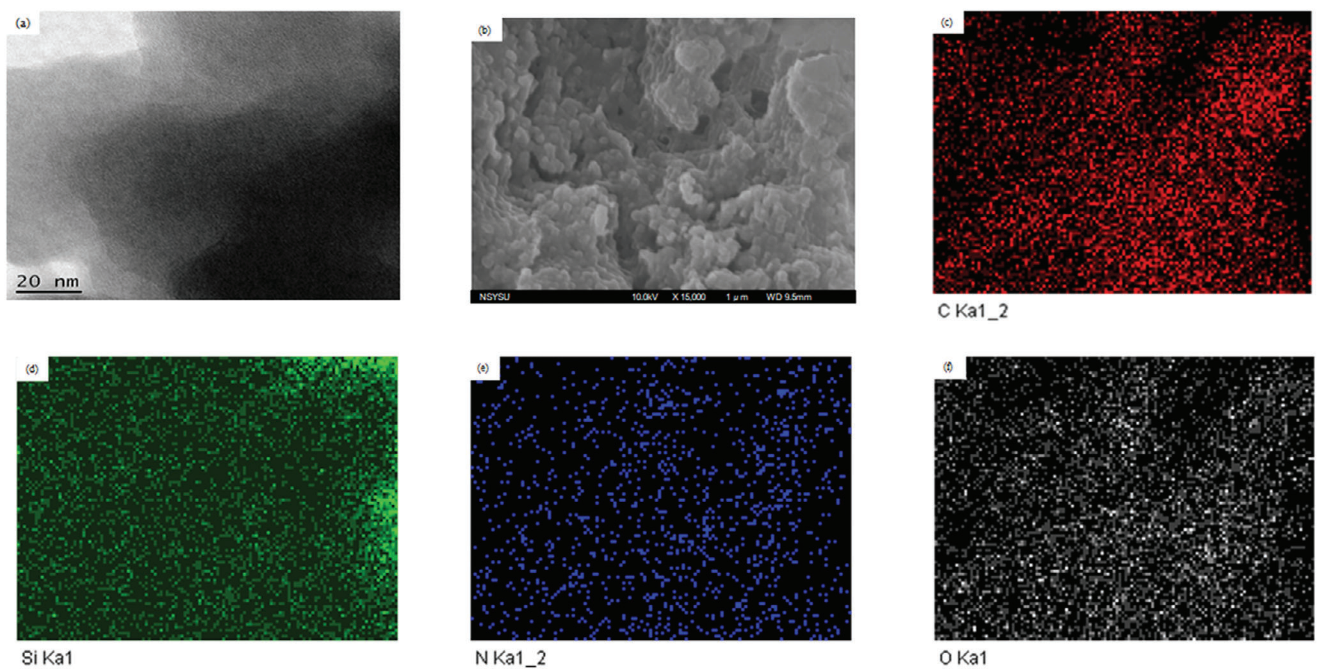

Figure 5. a) Transmission electron microscopy (TEM) and b) scanning electron microscopy (SEM) images and c–f) corresponding c) C–, d) Si–, e) N–, and f) O-mappings of PDMS-DABZ-DDSQ after thermal polymerization at 250 °C.

Macromolecular Rapid Communications
www.mrc-journal.de

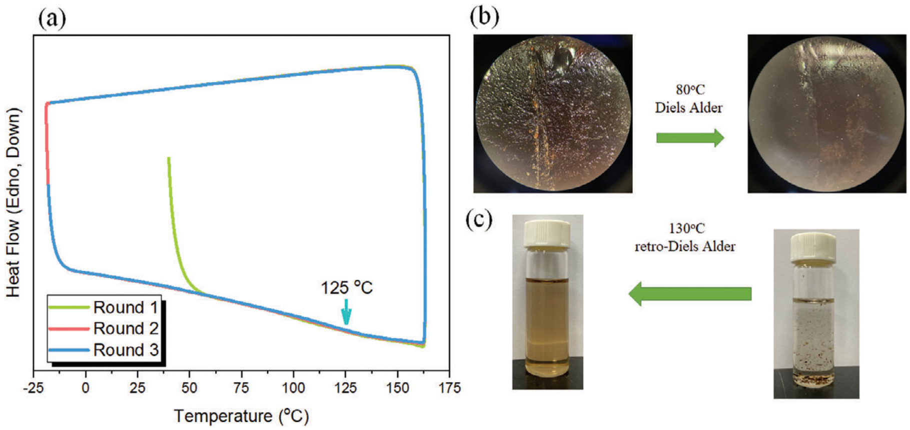

Figure 6. Reversible properties of PDMS-DABZ-DDSQ revealed through a) three cycles of differential scanning calorimetry (DSC) thermal analyses, b) a photograph of the self-healing behavior of the PDMS-DABZ-DDSQ prepolymer at 80 °C, and c) the PDMS-DABZ-DDSQ prepolymer dissolving in DMF after the reverse reaction had occurred at 130 °C.

lower than those of the poly(PDMS-FBZ) prior to complete thermal ROP (at temperatures of up to 200 °C), presumably because the inorganic DDSQ units imparted additional hydrophobicity. After complete thermal ROP at 250 °C, the surface free energy of the poly(PDMS-DABZ-DDSQ) film was slightly higher than those of poly(PDMS-FBZ) and BA-m–type PBZ films, presumably because of the presence of polar DA adducts; the value was, however, still lower than that of the typical BA-a–type PBZ.

Figure S6 (Supporting Information) displays the TGA thermograms of the poly(PDMS-FBZ) and poly(PDMS-DABZ-DDSQ) hybrids after thermal ROP at 250 °C and after continuing TGA heating at 250 °C for various period of time. We conclude that the incorporation of inorganic DDSQ units in PDMS-FBZ improved its thermal stability, with the char yield of the poly(PDMS-DABZ-DDSQ) hybrid (93.5 wt%) being higher than that of poly(PDMS-FBZ) (91.6 wt%) after 1 day at 250 °C. Furthermore, we used DSC to examine the reversible properties resulting from the DA reaction. When we increased the temperature to 160 °C and then back to –20 °C, the appearance of the broad complex endothermic signal near 125 °C, corresponding to the retro-DA reaction, was repeated for three rounds (**Figure 6**a). Most interestingly, this new PDMS-DABZ-DDSQ copolymer exhibited spontaneously reversible properties at 130 °C, indicating its possible use as an autonomously reversible material without the need for external intervention, as displayed in Figure 6b; furthermore, it could dissolve in DMF (Figure 6c) after the retro-DA reaction, but was insoluble after the DA reaction when the temperature was higher than 80 °C.[41,52–58]

3. Conclusions

We have used DA reactions to synthesize a highly thermal stable, flexible, low-surface-free-energy, and self-healing PBZ hybrid featuring both inorganic PDMS and DDSQ units. The high thermal stability of the PDMS-DABZ-DDSQ copolymer hybrid after thermal ROP was revealed by its values of T_g (177 °C) and T_{d10} (441 °C) and char yield (60.1 wt%) being much higher than those of the typical Pa-type BZ; its lower thermal ROP temperature, higher flexibility, and reversible properties arose because its main chain-type inorganic PDMS and DDSQ units were dispersed well in the PBZ matrix and because of the reversible nature of its DA and retro-DA reactions. Accordingly, this new main chain-type copolymer functions as a high-performance PBZ.

Supporting Information

Supporting Information is available from the Wiley Online Library or from the author.

Acknowledgements

This study was supported financially by the National Science and Technology Council, Taiwan, under contracts NSTC110-2811-E-110-002 and NSTC-111-2223-E-110-004.

Conflict of Interest

The authors declare no conflict of interest.

Data Availability Statement

The data that support the findings of this study are available from the corresponding author upon reasonable request.

Keywords

DDSQ, Diels–Alder, polybenzoxazine, polydimethylsiloxane, thermal property

Received: November 21, 2022
Revised: February 24, 2023
Published online: April 11, 2023

[1] H. Ishida, *Handbook of Polybenzoxazine Resins* (Eds: H. Ishida, T. Agag), Elsevier, Amsterdam **2011**, Ch. 1, pp. 3–81.

[2] K.-C. Chen, H.-T. Li, S.-C. Huang, W.-B. Chen, K.-W. Sun, F.-C. Chang, *Polym. Int.* **2011**, *60*, 1089.
[3] M. G. Mohamed, S.-W. Kuo, *Macromolecules* **2020**, *53*, 2420.
[4] M. G. Mohamed, T.-C. Chen, S.-W. Kuo, *Macromolecules* **2021**, *54*, 5866.
[5] M. G. Mohamed, C.-J. Li, M. A. R. Khan, C.-C. Liaw, K. Zhang, S.-W. Kuo, *Macromolecules* **2022**, *55*, 3106.
[6] R.-C. Lin, M. G. Mohamed, S.-W. Kuo, *Macromol. Rapid Commun.* **2017**, *38*, 1700251.
[7] J. Dunkers, E. A. Zarate, H. Ishida, *J. Phys. Chem.* **1996**, *100*, 13514.
[8] G. R. Goward, D. Sebastiani, I. Schnell, H. W. Spiess, H.-D. Kim, H. Ishida, *J. Am. Chem. Soc.* **2003**, *125*, 5792.
[9] H. Y. Low, H. Ishida, *J. Polym. Sci., Part B: Polym. Phys.* **1998**, *36*, 1935.
[10] H. J. Kim, Z. Brunovska, H. Ishida, *Polymer* **1999**, *40*, 6565.
[11] T. Agag, T. Takeichi, *Macromolecules* **2003**, *36*, 6010.
[12] Y. Xing, X. He, R. Yang, K. Zhang, S. Yang, *Polymers* **2020**, *12*, 2794.
[13] W.-H. Hu, K.-W. Huang, C.-W. Chiou, S.-W. Kuo, *Macromolecules* **2012**, *45*, 9020.
[14] W.-C. Chen, S.-W. Kuo, *Macromolecules* **2018**, *51*, 9602.
[15] A. Hariharan, K. Srinivasan, C. Murthy, M. Alagar, *Ind. Eng. Chem. Res.* **2017**, *56*, 9347.
[16] H. Gou, Y. Bao, J. Huang, X. Fei, X. Li, W. Wei, *Macromol. Mater. Eng.* **2022**, *307*, 2200351.
[17] M. G. Mohamed, S. W. Kuo, *Macromol. Chem. Phys.* **2019**, *220*, 1800306.
[18] M.-C. Tseng, Y.-L. Liu, *Polymer* **2010**, *51*, 5567.
[19] Y. Zhao, M. Yuan, L. Wang, X. Lu, Z. Xin, *Maromol. Mater. Eng.* **2022**, *307*, 2100747.
[20] K. Zhang, Q. Zhuang, X. Liu, G. Yang, R. Cai, Z. Han, *Macromolecules* **2013**, *46*, 2696.
[21] Y.-T. Liao, Y.-C. Lin, S.-W. Kuo, *Macromolecules* **2017**, *50*, 5739.
[22] N. Liu, L. Li, L. Wang, S. Zheng, *Polymer* **2017**, *109*, 254.
[23] L. Dumas, L. Bonnaud, M. Olivier, M. Poorteman, P. Dubois, *Chem. Commun.* **2013**, *49*, 9543.
[24] M. G. Mohamed, K.-C. Hsu, S.-W. Kuo, *Polym. Chem.* **2015**, *6*, 2423.
[25] M. M. Samy, M. G. Mohamed, S.-W. Kuo, *Compos. Sci. Tech.* **2020**, *199*, 108360.
[26] D. Ahn, H.-J. Choi, H.-D. Kim, S. Y. Yeo, *Polymers* **2020**, *12*, 179.
[27] S. M. Alhassan, S. Qutubuddin, D. A. Schiraldi, T. Agag, H. Ishida, *Eur. Polym. J.* **2013**, *49*, 3825.
[28] M. Zeng, J. Wang, R. Li, J. Liu, W. Chen, Q. Xu, Y. Gu, *Polymer* **2013**, *54*, 3107.
[29] A. A. Alhwaige, S. M. Alhassan, M. S. Katsiotis, H. Ishida, S. Qutubuddin, *RSC Adv.* **2015**, *5*, 92719.
[30] K. Sethuraman, M. Alagar, *RSC Adv.* **2015**, *5*, 9607.
[31] Y. Yagci, B. Kiskan, N. N. Ghosh, *J. Polym. Sci., Part A: Polym. Chem.* **2009**, *47*, 5565.
[32] M. Arslan, B. Kiskan, Y. Yagci, *Macromolecules* **2018**, *51*, 10095.
[33] I. Machado, E. Rachita, E. Fuller, V. M. A. Calado, H. Ishida, *ACS Sustainable Chem. Eng.* **2021**, *9*, 16637.
[34] T. Takeichi, R. Zeidam, T. Agag, *Polymer* **2002**, *43*, 45.
[35] H.-K. Fu, C.-F. Huang, S.-W. Kuo, H.-C. Lin, D.-R. Yei, F.-C. Chang, *Macromol. Rapid Commun.* **2008**, *29*, 1216.
[36] B. Kiskan, B. Aydogan, Y. Yagci, *J. Polym. Sci., Part A: Polym. Chem.* **2009**, *47*, 804.
[37] M. G. Mohamed, S.-W. Kuo, *Soft Matter* **2022**, *18*, 5535.
[38] S.-W. Kuo, *J. Polym. Res.* **2022**, *29*, 69.
[39] M. Mohamed, S.-W. Kuo, *Polymers* **2016**, *8*, 225.
[40] W.-C. Chen, Z.-Y.u Chen, Y. Ba, B. Wang, G. Chen, X. Fang, S.-W. Kuo, *Polymers* **2022**, *14*, 2380.
[41] K. Zhang, Y. Liu, H. Ishida, *Macromolecules* **2019**, *52*, 7386.
[42] P. Froimowicz, C. R. Arza, L. Han, H. Ishida, *ChemSusChem* **2016**, *9*, 1921.
[43] J. Dai, N. Teng, Y. Peng, Y. Liu, L. Cao, J. Zhu, X. Liu, *ChemSusChem* **2018**, *11*, 3175.
[44] C.-F. Wang, Y.-C. Su, S.-W. Kuo, C.-F. Huang, Y.-C. Sheen, F.-C. Chang, *Angew. Chem., Int. Ed.* **2006**, *45*, 2248.
[45] S.-W. Kuo, Y.-C. Wu, C.-F. Wang, K.-U. Jeong, *J. Phys. Chem. C.* **2009**, *113*, 20666.
[46] L. Wang, W. Gong, S. Zheng, *Polym. Int.* **2009**, *58*, 124.
[47] L. Wang, S. Zheng, *Polymer* **2010**, *51*, 1124.
[48] C.-I. Chou, Y.-L. Liu, *J. Polym. Sci., Part A: Polym. Chem.* **2008**, *46*, 6509.
[49] Q. Tian, Y. C. Yuan, M. Z. Rong, M. Q. Zhang, *J. Mater. Chem.* **2009**, *19*, 1289.
[50] M. Shibata, N. Teramoto, T. Akiba, M. Ogihara, *Polymer J.* **2011**, *43*, 455.
[51] P. Du, X. Liu, Z. Zheng, X. Wang, T. Joncheray, Y. Zhang, *RSC Adv.* **2013**, *3*, 15475.
[52] Y. Zhang, A. A. Broekhuis, F. Picchioni, *Macromolecules* **2009**, *42*, 1906.
[53] H. Weizman, C. Nielsen, O. S. Weizman, S. Nemat-Nasser, *J. Chem. Educ.* **2011**, *88*, 1137.
[54] P. A. Pratama, M. Sharifi, A. M. Peterson, *G. R. Palmese, ACS Appl. Mater. Interfaces* **2013**, *5*, 12425.
[55] X. Kuang, G. Liu, X. Dong, X. Liu, J. Xu, D. Wang, *J. Polym. Sci., Part A: Polym. Chem.* **2015**, *53*, 2094.
[56] Y. Y. Jo, A. S. Lee, K.-Y. Baek, H. Lee, S. S. Hwang, *Polymer* **2017**, *108*, 58.
[57] S. Terryn, J. Brancart, E. Roels, R. Verhelle, A. Safaei, A. Cuvellier, B. Vanderborght, G. van Assche, *Macromolecules* **2022**, *55*, 5497.
[58] P. Berto, J. Mehats, A.-L. Wirotius, S. Grelier, F. Peruch, *Macromolecules* **2022**, *55*, 4557.